Two-phase flow measurements in turbulent hydraulic jumps

F. Murzyn [a], H. Chanson [b],*

[a] ESTACA Campus Ouest, Parc Universitaire de Laval-Changé, Rue Georges Charpak, BP 76121, 53061 Laval Cedex 9, France
[b] Division of Civil Engineering, The University of Queensland, Brisbane, Qld 4072, Australia

ABSTRACT

Hydraulic jumps are commonly experienced in industrial applications and manufacturing processes, as well in rivers and canals. The hydraulic jump is the sudden transition from a high-velocity open channel flow to a subcritical flow motion. Despite nearly two centuries of studies, there is still a lack of knowledge on the two-phase flow properties of the turbulent shear layer and the roller. New series of experimental measurements were conducted in hydraulic jumps with Froude numbers between 5 and 8.5, and inflow Reynolds numbers between 38,000 and 62,000. The two-phase flow measurements included some vertical profiles of void fraction, bubble count rate, interfacial velocity and bubble chords. In the air–water shear region, the void fraction and bubble count rate distributions exhibited marked peaks, with the maximum of void fraction always above the location of the maximum bubble count rate. The dimensionless turbulent diffusivity coefficient was estimated. The dimensionless distributions of interfacial velocity compared favourably with some wall-jet flow equations. The data analysis showed that the mean bubble chord in the turbulent shear layer was between 1 mm and 6 mm. The probability distribution functions (PDF) of bubble chord time illustrated a broad spectrum with predominance to small bubbles compared to the mean.

© 2008 The Institution of Chemical Engineers. Published by Elsevier B.V. All rights reserved.

Keywords: Hydraulic jumps; Two-phase flow properties; Developing shear layer; Void fraction; Bubble count rate; Air bubble diffusion

1.   Introduction

The hydraulic jump is the sudden transition from a high-velocity open channel flow to a subcritical flow motion. Hydraulic jumps are commonly experienced in industrial applications and manufacturing processes, in rivers and canals, as well as in the kitchen sink. For chemical engineering and environmental applications (water treatment, pollutant dispersion, etc.), hydraulic jumps are common turbulent flows particularly characterised by strong mixing properties. For a horizontal rectangular channel and neglecting boundary friction, the continuity and momentum principles give a series of relationships between the upstream and downstream flow properties (Belanger, 1828):

$$\frac{d_2}{d_1} = \frac{1}{2} \times (\sqrt{1 + 8 \times Fr_1^2} - 1) \qquad (1)$$

$$\frac{Fr_2}{Fr_1} = \frac{2^{3/2}}{\left(\sqrt{1 + 8 \times Fr_1^2} - 1\right)^{3/2}} \qquad (2)$$

where the subscripts 1 and 2 refer to the upstream and downstream flow conditions respectively, Fr is the Froude number: $Fr = V/\sqrt{g \times d}$, d and V are the flow depth and velocity respectively, and g is the gravity acceleration. The hydraulic jump is typically classified in terms of its inflow Froude number Fr_1 that is always greater than unity (Belanger, 1828; Henderson, 1966; Chanson, 2004). For a Froude number slightly above unity, the hydraulic jump presents a smooth rise of the free-surface followed by a train of stationary free-surface undulations. For larger Froude numbers, the jump is characterised by a marked roller, some highly turbulent motion with macro-scale vortices, significant kinetic energy dissipation and a bubbly two-phase flow region (Fig. 1).

Nomenclature

C	void fraction defined as the volume of air per unit volume of air
C_{max}	maximum void fraction in the air bubble diffusion layer
d	flow depth (m)
d_1	flow depth (m) measured perpendicular to the flow direction at the upstream gate
d_2	flow depth (m) measured perpendicular to the flow downstream of the hydraulic jump
D_t	turbulent diffusivity (m^2/s) of air bubbles in air–water flow
D^*	dimensionless turbulent diffusivity: $D^* = D_t/V_1 \times d_1$
F	bubble count rate (Hz), or bubble frequency (number of detected air bubbles per unit time)
F_{max}	maximum bubble count rate (Hz) at a given cross-section
Fr_1	upstream Froude number: $Fr_1 = V_1/\sqrt{g \times d_1}$
Fr_2	downstream Froude number: $Fr_2 = V_2/\sqrt{g \times d_2}$
g	gravity constant: $g = 9.80$ m/s^2 in Brisbane, Australia
N	inverse of the exponent of the velocity power law
N_{ab}	number of air bubbles per record
q	water discharge per unit width (m^2/s);
Q	water discharge (m^3/s)
Re	Reynolds number: $Re = \rho \times V_1 \times d_1/\mu$
T	average air–water interfacial travel time between the two probe sensors (s)
V	interfacial velocity (m/s)
V_{max}	maximum velocity (m/s) in the wall jet
V_1	depth-averaged flow velocity upstream the hydraulic jump (m/s): $V_1 = q/d_1$
V_2	depth-averaged flow velocity downstream the hydraulic jump (m/s)
W	channel width (m)
x	longitudinal distance from the upstream gate (m)
x_1	longitudinal distance from the gate to the jump toe (m)
Δx	longitudinal distance (m) between probe sensors (dual-tip conductivity probe)
y	distance (m) measured normal to the channel bed
$y_{C_{max}}$	distance (m) normal to the jet support where $C = C_{max}$
$y_{F_{max}}$	distance (m) normal to the jet support where $F = F_{max}$
$y_{V_{max}}$	distance (m) from invert where $V = V_{max}$
$y_{0.5}$	distance (m) normal to invert where $V = V_{max}/2$

Greek symbols

μ	dynamic viscosity of water (Pa s)
ν	kinematic viscosity of water (m^2/s)
ρ	density (kg/m^3) of water

Subscripts

max	maximum
xx	auto-correlation of reference probe signal
1	upstream flow conditions
2	downstream flow conditions

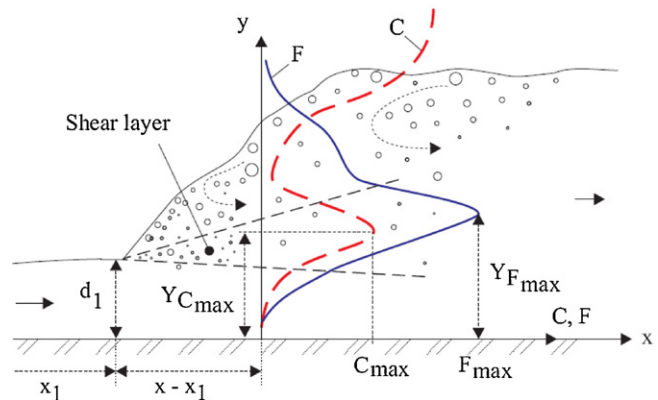**Fig. 1 – Air bubble entrainment in a hydraulic jump. (A) $Fr_1 = 8.45$, $d_1 = 0.018$ m, $x_1 = 0.75$ m, $Re = 6.4 \times 10^4$, shutter speed: 1/80 s. Note the dual-tip conductivity probe above the roller free-surface. (B) Definition sketch.**

The early investigations of air entrainment in hydraulic jumps focused on the quantity of entrained air in closed conduits (e.g. Kalinske and Robertson, 1943; Wisner, 1965). The first successful two-phase flow measurements in hydraulic jumps were performed by Rajaratnam (1962) and a significant contribution was the work of Resch and Leutheusser (1972). Further advances included several complementary studies by Chanson (1995), Mossa and Tolve (1998), Chanson and Brattberg (2000), Murzyn et al. (2005, 2007) and Chanson (2007) (Table 1). Despite these pertinent studies, relatively little information is available on the two-phase flow properties of turbulent hydraulic jumps.

The present contribution addresses a topic with a broad range of applications, including in the areas of energy with application in the nuclear engineering industry, water as a critical resource and for industrial usage, and bioprocess engineering with low environmental impact. This article aims to investigate the two-phase flow properties in hydraulic jumps with relatively large inflow Froude numbers ($5 < Fr_1 < 8.5$). New experiments were performed under controlled flow conditions using a phase-detection intrusive probe. The results yield an enhanced characterisation of the bubbly flow properties and turbulent mixing in hydraulic jumps.

2. Experimental methods and facilities

New experiments were performed in a horizontal rectangular flume at the Gordon McKay Hydraulics Laboratory of Univer-

Table 1 – Detailed air–water flow measurements in hydraulic jumps with partially developed inflow conditions.								
Reference	x_1 (m)	d_1 (m)	V_1 (m/s)	Fr_1	Re	W (m)	Instrumentation	Sampling
Resch and Leutheusser (1972)	–	0.039	1.89	2.85	73,200	0.39	Hot-film	2.5 kHz for 102.4 s
		0.012	2.80	6.0	33,400			
Chanson (1995)	0.70	0.016	1.97	5.02	31,300	0.25	Single-tip conductivity	Analog integration
	0.67	0.016	2.23	5.66	35,400		($\emptyset = 0.35$ mm)	(90 s)
	0.89	0.017	2.47	6.05	41,700			
	0.94	0.016	3.16	8.04	50,200			
	0.96	0.016	3.19	8.11	50,700			
Chanson and Brattberg (2000)	0.5	0.014	2.34	6.3	33,000	0.25	Dual-tip conductivity	20 kHz for 10 s
			3.14	8.5	44,000		($\emptyset = 0.025$ mm)	
Murzyn et al. (2005)	0.35	0.059	1.50	2.0	88,000	0.30	Dual-tip optical fibre	Less than 1 MHz for 120 s
		0.046	1.64	2.4	75,000		($\emptyset = 0.010$ mm)	
		0.032	2.05	3.7	65,000			
		0.021	2.19	4.8	46,000			
Gualtieri and Chanson (2007)	0.5	0.012–0.013	1.9–4.9	5.2–14.3	24,700–58,000	0.25	Single-tip conductivity	20 kHz for 45 s
							($\emptyset = 0.35$ mm)	
Chanson (2007)	1.0	0.024	2.6	5.1	68,000	0.5	Single-tip conductivity	20 kHz for 45 s
			4.15	8.6	98,000		($\emptyset = 0.35$ mm)	
Present study								
Run 1	0.75	0.018	2.12	5.1	38,150	0.50	Dual-tip conductivity	20 kHz for 45 s
Run 2		0.018	3.18	7.6	57,250		($\emptyset = 0.25$ mm)	
Run 3		0.018	3.47	8.3	62,250			

Table 2 – Characteristic properties of void fraction bubble count rate and interfacial velocity distributions in hydraulic jumps.

Run	Fr_1	d_1 (m)	x_1/d_1	$(x-x_1)/d_1$	C_{max}	$y_{C_{max}}/d_1$	$F_{max} \times d_1/V_1$	$y_{F_{max}}/d_1$	V_{max}/V_1	$y_{V_{max}}/d_1$
1	5.1	0.018	41.7	4.17	0.218	1.67	0.47	1.50	0.80	0.17
				8.33	0.175	2.17	0.37	1.67	0.75	1.00
				12.50	0.063	2.00	0.22	1.67	0.53	1.83
2	7.6	0.018	41.7	12.50	0.208	2.11	0.55	1.50	0.70	1.00
				16.67	0.167	2.17	0.47	2.00	0.64	1.33
				25.00	0.083	2.83	0.28	1.83	0.58	0.67
3	8.3	0.018	41.7	12.50	0.28	2.17	0.65	1.50	0.81	0.67
				16.67	0.212	2.50	0.55	1.83	0.75	0.67
				25.00	0.118	3.22	0.37	1.83	0.65	0.72
				33.33	0.073	4.11	0.25	2.39	0.52	1.83

sity of Queensland (Fig. 1). The channel width was 0.50 m. The sidewall height and flume length were respectively 0.45 m and 3.2 m. The sidewalls were made of glass and the channel bed was PVC. This channel was previously used by Chanson (2005a, 2007). Further details on the experimental facility were reported in Murzyn and Chanson (2007).

The water discharge was measured with a Venturi meter located in the supply line and which was calibrated on-site with a large V-notch weir. The discharge measurement was accurate within $\pm 2\%$. The clear-water flow depths were measured using rail mounted point gages with a 0.2 mm accuracy. The upstream gate aperture was fixed during all experiments ($d_1 = 0.018$ m).

The two-phase flow properties were measured with a double-tip conductivity probe seen in Fig. 1A. The probe was equipped with two identical sensors with an inner diameter of 0.25 mm. The streamwise distance between probe tips was $\Delta x = 7.0$ mm. The probe was manufactured at the University of Queensland. It was previously used in several studies, including Chanson (2005b) and Chanson and Carosi (2007). The dual-tip probe was excited by an electronic system (Ref. UQ82.518) designed with a response time of less than 10 μs. During the experiments, each probe sensor was sampled at 20 kHz for 45 s and the recorded output signal was a voltage ranging from 0 (air) to 4.5 V (water) (Fig. 2). Depending upon the upstream Froude number, three to four vertical profiles were recorded at different cross-sections downstream of the jump toe (Table 2). Each vertical profile contained at least 30 points. The displacement and the position of the probe in the vertical direction were controlled by a fine adjustment system

connected to a Mitutoyo™ digimatic scale unit with a vertical accuracy Δy of less than 0.1 mm.

The analysis of the probe voltage output was based upon a single threshold technique with a threshold set between 45% and 55% of the air–water voltage range. Below this threshold, the probe sensor was in air whereas it was in water for larger voltage output voltages (Fig. 2). The error on the void fraction was expected to be less than 1% using this technique.

The signal analysis yielded a number of two-phase flow properties including the void fraction C, the bubble count rate F defined as the number of bubbles impacting the probe tip per second, and the air chord time distribution where the chord time is defined as the time spent by the bubble on the probe tip. The interfacial velocities V were estimated as

$$V = \frac{\Delta x}{T} \tag{3}$$

where Δx is the longitudinal distance between both tips ($\Delta x = 7.0$ mm herein) and T is the average air-water interfacial time between the two probe sensors that was deduced from a cross-correlation analysis (Crowe et al., 1998; Chanson, 1997, 2002). Note that Eq. (3) implies that both probe sensors are aligned along a streamline. This assumption is correct in the shear flow region, but it becomes meaningless in the recirculation region of the hydraulic jump roller.

2.1. Experimental flow conditions

The foot of the jump, or jump toe, was always fixed at $x_1 = 0.75$ m where x_1 is the distance from the upstream gate (Table 1). All sets of experiments were carried out with the same upstream rounded gate opening $d_1 = 0.018$ m. This was taken as the upstream flow depth since the gate contraction coefficient was basically unity. For that configuration, the hydraulic jump inflow was characterised by a partially developed boundary layer (Chanson, 2005a).

A summary of the flow conditions is given in Tables 1 and 2, where x_1 is the position of the toe downstream of the upstream gate and Re is the Reynolds number defined as

$$Re = \rho \frac{V_1 d_1}{\mu} \tag{4}$$

with ρ and μ being the density and dynamic viscosity of water respectively. In Table 2, $x - x_1$ is the longitudinal position downstream of the toe where the vertical profiles were measured (Fig. 1B).
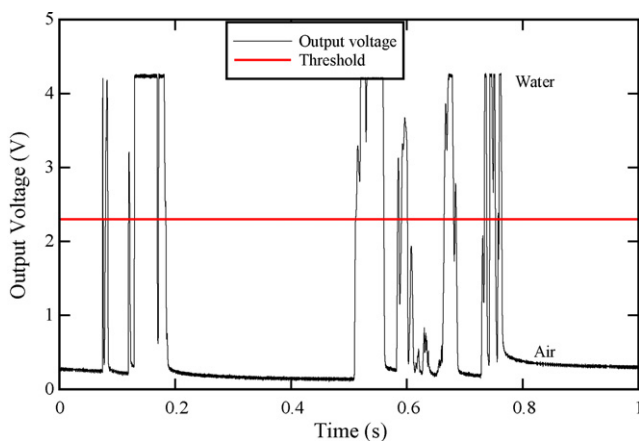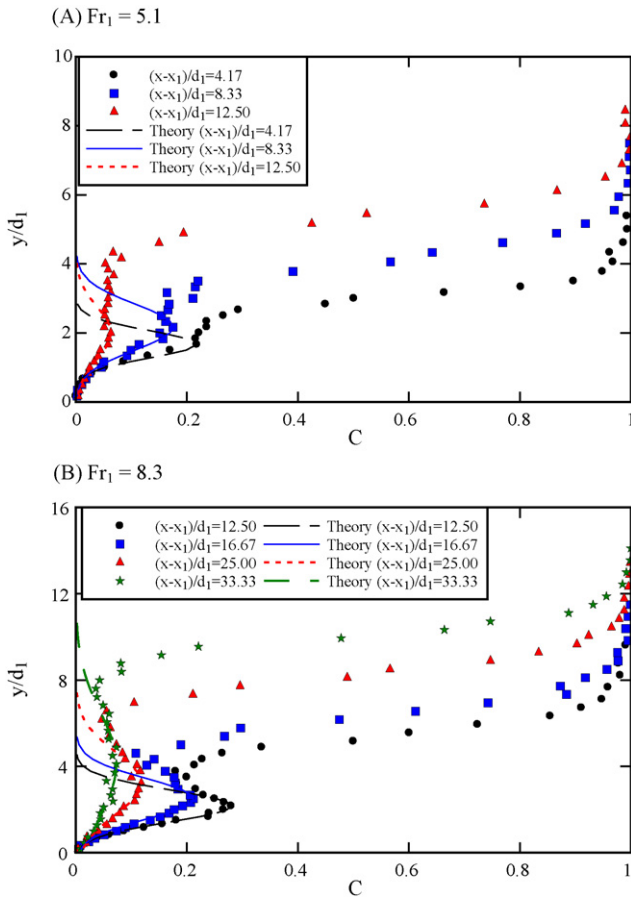

Fig. 2 – Typical signal output of a conductivity probe sensor with a single threshold. Flow conditions: $Fr_1 = 5.1$, $d_1 = 0.018$ m, $x - x_1 = 0.09$ m, $y = 0.083$ m, $C = 0.19$, $F = 14$ Hz.

(A) $Fr_1 = 5.1$

(B) $Fr_1 = 8.3$

Fig. 3 – Dimensionless distributions of void fraction along the hydraulic jump. Comparison with Eq. (5). (A) $Fr_1 = 5.1$. (B) $Fr_1 = 8.3$.

3. Experimental results and analyses

3.1. Distributions of void fractions and bubble count rate

In hydraulic jumps, air bubble entrainment occurred at the intersection of the supercritical flow with the roller. Bubbles and air packets were entrained at the flow singularity formed by the impingement point (Fig. 1). These were dispersed and advected downstream in a turbulent shear flow. In the jump roller, two regions were identified. The lower part was dominated by the developing turbulent shear layer where air bubbles were broken up into small bubbles and entrained in this high shear stress region. Above the mixing layer, the recirculation and upper flow region was characterized by large air contents, splashes and recirculation areas, with large eddies and a wavy free surface pattern.

For $Fr_1 = 5.1–8.3$, vertical profiles of void fractions were measured at different longitudinal positions $4.1 < (x - x_1)/d_1 < 34$ (Table 2). Fig. 3 presents some typical results. In the developing shear layer, the data compared favourably with an analytical solution of the advective diffusion equation for air bubbles (Chanson, 1997):

$$C = C_{max} \exp\left(-\frac{((y - y_{C_{max}})/d_1)^2}{4 \times D^* \times ((x - x_1)/d_1)} \right) \quad (5)$$

where C_{max} is the maximum void fraction in the shear layer, $y_{C_{max}}$ is the vertical elevation of the maximum void

fraction C_{max}, D^* is a dimensionless turbulent diffusivity: $D^* = D_t/(V_1 \times d_1)$, D_t is the air bubble turbulent diffusivity. Eq. (5) was developed within a series of basic assumptions including negligible compressibility effects, $\partial C/\partial x \ll \partial C/\partial y$, a diffusivity $D^\#$ independent of the transverse coordinate y, and an uniform velocity distribution (Chanson, 1997). While some assumptions might not be truly applicable, Fig. 3 showed a good agreement between Eq. (5) and experimental observations in the developing shear region. Such a good agreement between Eq. (5) and experimental data was previously observed in hydraulic jumps with partially developed inflow conditions, including a re-analysis of the data of Resch and Leutheusser (1972) and Chanson (1995), and the newer studies of Chanson and Brattberg (2000), Murzyn et al. (2005), Chanson (2007) and Gualtieri and Chanson (2007).

The peak of void fraction C_{max} was clearly marked for all investigated conditions (Fig. 3). At a given position downstream of the toe, C_{max} increased with increasing Froude number while, for a given Froude number, it decreased with the distance from the jump toe. The present data are shown in Fig. 4 and summarised in Table 2. A good agreement was observed with the correlation of Kucukali and Chanson (2007):

$$C_{max} = 0.07 \times Fr_1 \exp\left(-0.064 \frac{x - x_1}{d_1} \right) \quad (6)$$

(A) Maximum void fraction C_{max} - Comparison with Equation (6)

(B) Dimensionless location $y_{C_{max}}/d_1$ - Comparison with the correlation of CHANSON and BRATTBERG (2000)
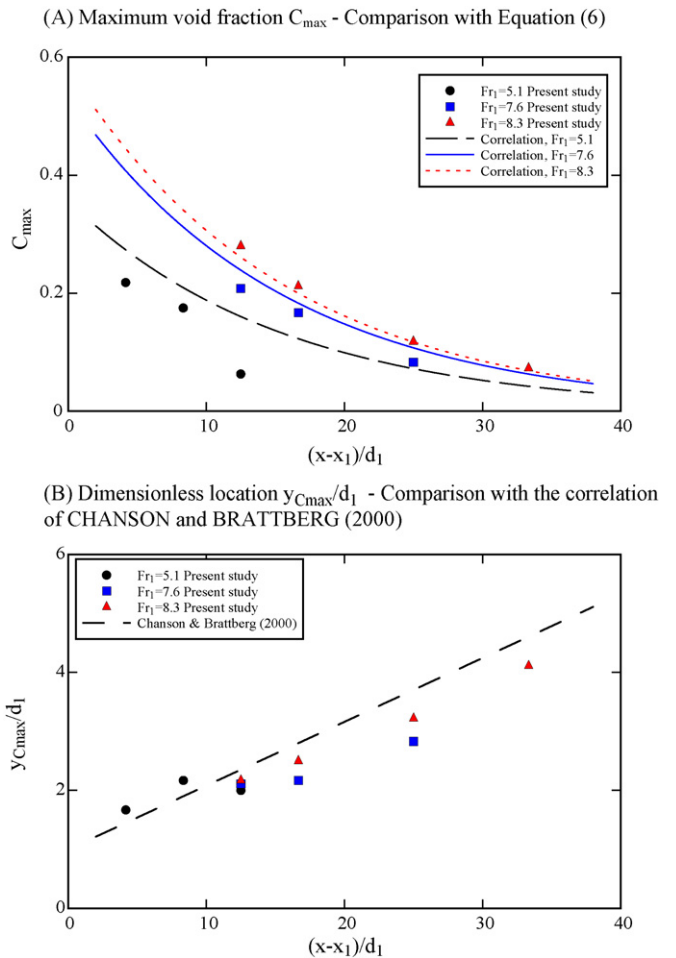

Fig. 4 – Characteristic properties of the maximum void fraction in the developing shear layer. (A) Maximum void fraction C_{max}. Comparison with Eq. (6). (B) Dimensionless location $y_{C_{max}}/d_1$. Comparison with the correlation of Chanson and Brattberg (2000).
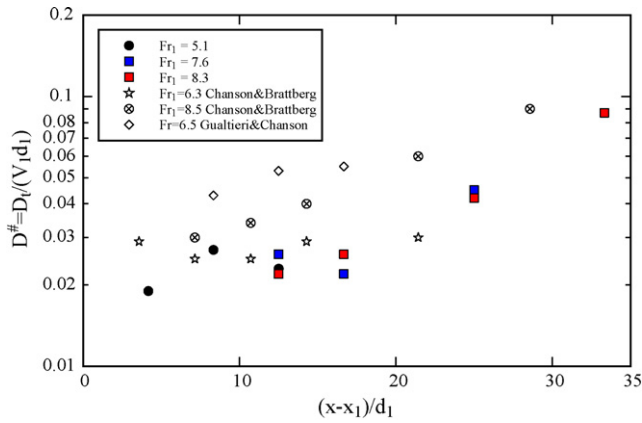
Fig. 5 – Dimensionless turbulent diffusivity coefficient D^* in the hydraulic jump shear layer. Comparison with experimental results by Chanson and Brattberg (2000) and Gualtieri and Chanson (2007).

Eq. (6) is compared with the present data in Fig. 4A. For a given Froude number, the vertical elevation of the maximum void fraction $y_{C_{max}}/d_1$ increased with increasing distance from the toe (Fig. 4B). This was linked with some buoyancy effects inducing some bubble de-aeration. The present results compared well with the findings of Chanson and Brattberg (2000):

$$\frac{y_{C_{max}}}{d_1} = 1 + 0.11 \frac{x - x_1}{d_1} \qquad (7)$$

Eq. (7) was compared successfully with a range of studies and it is shown in Fig. 4B.

From a practical point of view, in chemical, industrial and environmental engineering science, the turbulent diffusivity is a relevant design parameter for an accurate prediction of particle dispersion. The dimensionless turbulent diffusivity in hydraulic jumps was deduced for $5.1 < Fr_1 < 8.3$ from the best fit of the vertical void fraction profiles in the developing shear layer. The results in terms of D^* are presented in Fig. 5 as a function of the dimensionless distance to the jump toe, and they are compared with earlier observations by Chanson and Brattberg (2000) and Gualtieri and Chanson (2007). They showed a comparable order of magnitude and a similar trend: i.e., the diffusivity data increased with increasing distance to the jump toe (Fig. 5), despite some basic differences in experimental techniques and instrumentation data sets between these studies (Table 1).
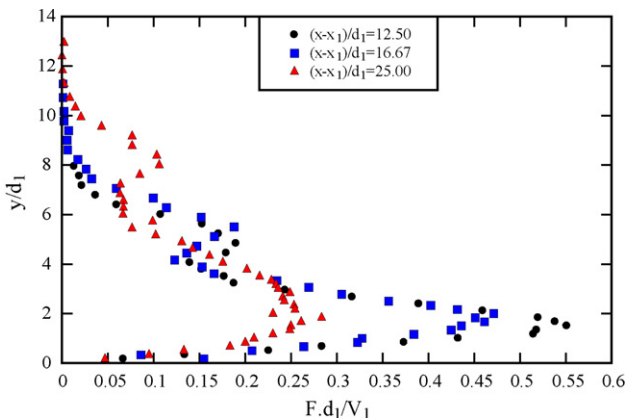

Fig. 6 – Dimensionless distributions of bubble count rate $F \times d_1/V_1$ in the hydraulic jump roller for $Fr_1 = 7.6$.
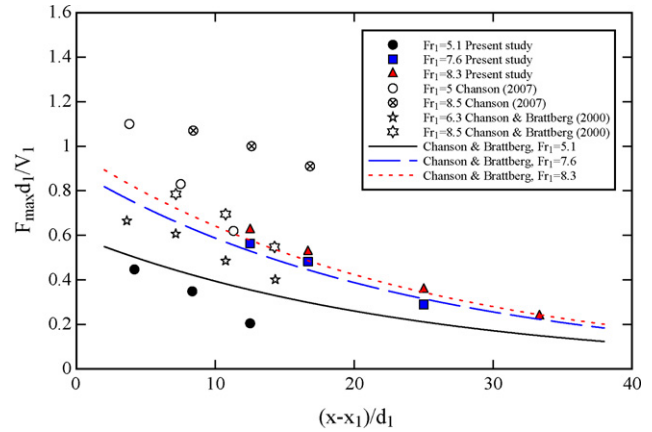

Fig. 7 – Dimensionless maximum bubble count rate in the hydraulic jump shear layer $F_{max} \times d_1/V_1$. Comparison with the data of Chanson and Brattberg (2000) and Chanson (2007), and with Eq. (8).

Fig. 6 presents some typical vertical distributions of dimensionless bubble count rate $F \times d_1/V_1$. The bubble count rate F, defined the number of bubbles detected by the probe sensor per unit time, is proportional to the specific gas–liquid interface area. All the data exhibited a major peak of bubble count rate F_{max} in the developing shear region. This feature was previously documented by Chanson and Brattberg (2000), Murzyn et al. (2005), Chanson (2007) and Gualtieri and Chanson (2007). It is believed that this maximum bubble count rate was linked with high turbulent shear stresses in the shear region that break up the entrained air bubbles into finer particles. The maximum bubble count rate F_{max} increased with increasing Froude number. For $Fr_1 = 5.1$, F_{max} reached 55 Hz whereas it was nearly 124 Hz for $Fr_1 = 8.3$ (Table 2). For a given Froude number, F_{max} decreased with an increasing distance from the impingement point as shown in Fig. 6 and reported in Table 2.

The dimensionless maximum bubble count rates $F_{max} \times d_1/V_1$ were compared with earlier results (Fig. 7). The data showed consistently a longitudinal decay in maximum bubble count rate with increasing dimensionless distance downstream of the jump toe. Some data scatter is noted in Fig. 7 that might be related to some difference in instrumentation and probe sensor sizes (Table 1). The present data however agreed well with the experimental results of Chanson and Brattberg (2000), and their empirical correlation:

$$\frac{F_{max} d_1}{V_1} = 0.117 \times Fr_1 \exp\left(-0.0415 \frac{x - x_1}{d_1}\right) \qquad (8)$$

Eq. (8) is compared with the present data in Fig. 7.

Importantly, the present results highlighted that the location of maximum bubble count rate F_{max} was always observed below the location of maximum void fraction C_{max} in the shear layer such that:

$$1 < \frac{y_{F_{max}}}{d_1} < \frac{y_{C_{max}}}{d_1} \qquad (9)$$

This finding was first reported by Chanson and Brattberg (2000). Chanson (2007) argued that it is caused by a double diffusion process whereas vorticity and air bubbles diffuse at a different rate and in a different manner downstream of the impingement point. Eq. (9) is illustrated in Fig. 8 where $y_{F_{max}}/d_1$ is plotted as a function $y_{C_{max}}/d_1$ for a range of experimental data.
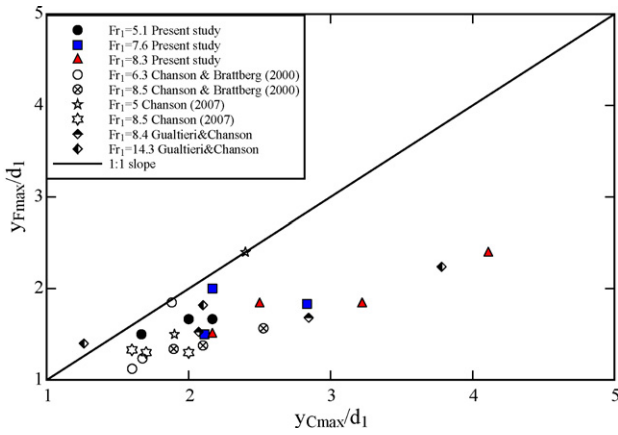
Fig. 8 – Dimensionless relationship between $y_{F_{max}}/d_1$ and $y_{C_{max}}/d_1$ in hydraulic jumps. Comparison between the present results and the data of Chanson and Brattberg (2000), Chanson (2007) and Gualtieri and Chanson (2007).

3.2. Bubble chord and chord time distributions

All the results showed some millimetric bubble chord sizes in the jump roller. Visual observations and high-shutter speed photography taken during experiments tended to confirm the findings. Some typical mean bubble chord length data are presented in Fig. 9. Note that the horizontal axes have dimensional units (mm), and the same scales are used for the horizontal and vertical axes in each graph. The results are limited to the mean bubbles chord lengths in the jump roller and measurements at large void fractions are not presented.
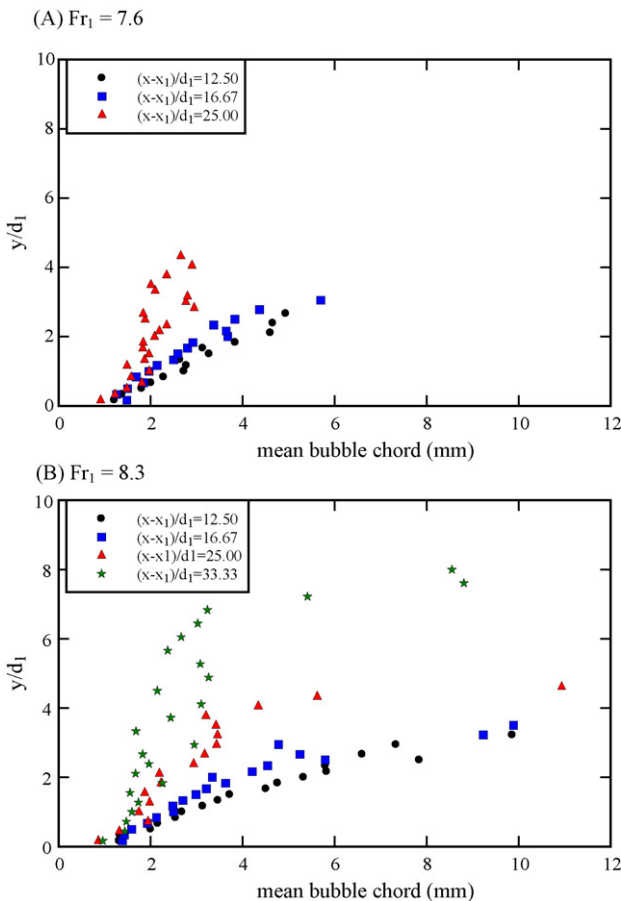

Fig. 9 – Vertical distributions of mean bubble chord length in the hydraulic jump roller. (A) $Fr_1 = 7.6$. (B) $Fr_1 = 8.3$.

The vertical distributions of mean bubble chords showed systematically an increase in mean bubble chord with increasing vertical elevation above the bed (Fig. 9). At a given position $(x - x_1)/d_1$, the smallest air bubbles were found close to the channel bed in regions of high shear. At a given elevation y/d_1, the mean bubble chord size decreased with increasing distance from the jump toe $(x - x_1)/d_1$. The order of magnitude of the present observations was in agreement with those published by Murzyn et al. (2005) and Chanson (2007). For example, Murzyn et al. (2005) reported Sauter mean diameter ranging from 2 mm to 10 mm in the developing shear layer for $Fr_1 = 2.0–4.8$.

Further information on the air–water flow structure included the probability density functions (PDF) of bubble chord times. The bubble chord time is defined as the time spent by the bubble on the probe tip. It is thus proportional to the bubble chord length and inversely proportional to the bubble velocity. Herein, the focus was on the PDFs of bubble chord time at two characteristic relative elevations ($y_{C_{max}}/d_1$ and $y_{F_{max}}/d_1$) corresponding respectively to the positions of maximum void fraction and bubble count rate in the developing shear layer (Fig. 1B). Typical results are presented in Fig. 10 where all the graphs have the same horizontal and vertical scales. For each graph, the caption and legend provide the location $(x - x_1, y/d_1)$, local air–water flow properties (C, F), and number of recorded bubbles N_{ab} while the horizontal axis lists the chord time interval in milliseconds. The histogram columns represent each the normalised probability of bubble chord time in a 0.5 ms chord time interval. For example, the probability of bubble chord time from 1 to 1.5 ms is represented by the column labelled 1. Bubble chord times larger than 15 ms are regrouped in the last column (>15).

The results highlighted the broad spectrum of bubble chord times at each location with a preponderance for small bubble chord times compared to the mean. The range extended from less than 0.5 ms to more than 15 ms. Further, when Froude number increased, the PDFs became more skewed with a longer upper chord size tail, and a larger proportion of small bubbles with increasing Froude number. Overall the findings were in agreement with the earlier experimental observations of Chanson (2007).

3.3. Distributions of interfacial velocity

Air–water velocity measurements were conducted with the dual-tip conductivity probe based upon the mean travel time between the probe sensors and the distance between both tips. The measurements were restricted to the air–water flow regions where the velocity was positive and the probe sensors were aligned with the flow streamlines. In the recirculation region, the results were meaningless because of negative velocities. Phase-detection probes, and hot-film probes, cannot differentiate between positive and negative instantaneous velocities.

Fig. 11 presents typical dimensionless distributions of interfacial velocities V/V_{max} in the hydraulic jump roller, where V_{max} is the maximum velocity measured in the cross-section. At the channel bed, the no-slip condition imposed $V(y = 0) = 0$. At a given longitudinal distance $(x - x_1)/d_1$, the velocity profiles showed the development of a boundary layer next to the bed. This thin fluid layer was characterised by a rapid increase in dimensionless interfacial velocity V/V_{max} from 0 for $y = 0$ to 1 at $y = y_{V_{max}}$. Above ($y > y_{V_{max}}$), a gradual decrease in velocity was observed (Fig. 11). All the velocity
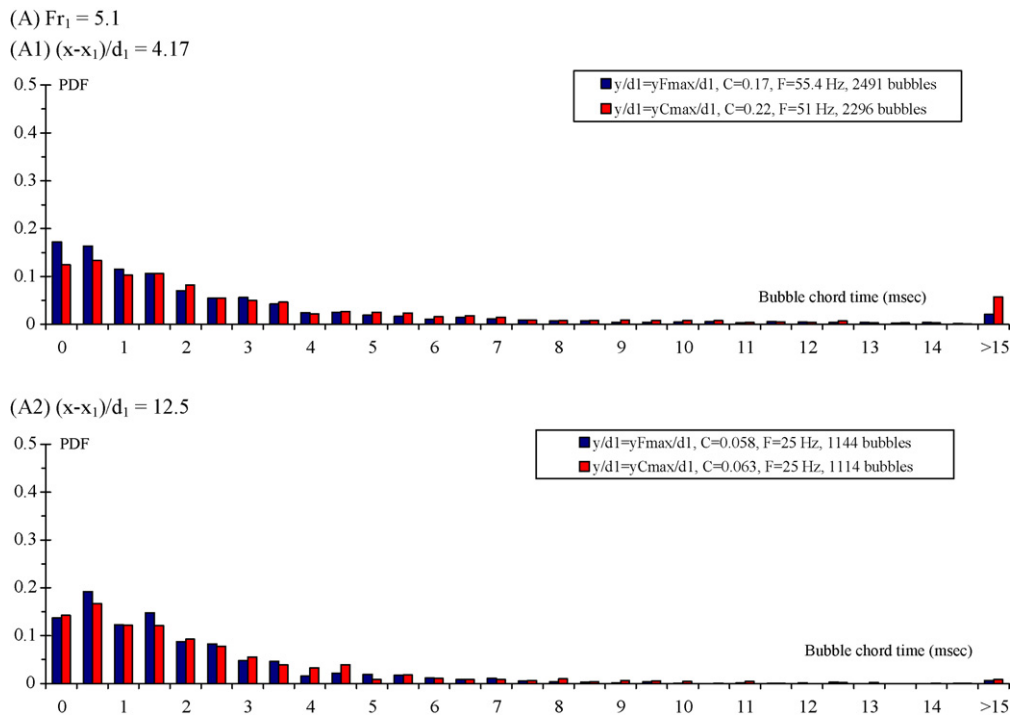
Fig. 10 – Bubble chord time distributions at two characteristic relative elevations ($y_{C_{max}}/d_1$ and $y_{F_{max}}/d_1$) in the bubbly flow region of hydraulic jumps. (A) $Fr_1 = 5.1$. (A1) $(x − x_1)/d_1 = 4.17$. (A2) $(x − x_1)/d_1 = 12.5$. (B) $Fr_1 = 8.3$. (B1) $(x − x_1)/d_1 = 12.5$. (B2) $(x − x_1)/d_1 = 25$.
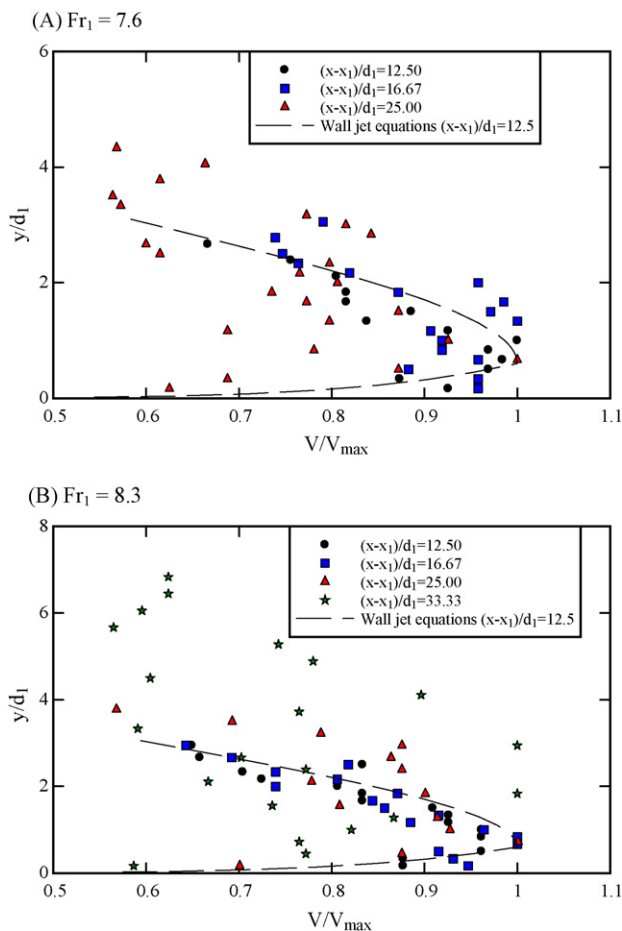

Fig. 11 – Dimensionless distributions of interfacial velocity V/V_{max} in hydraulic jumps. Comparison with Eqs. (10) and (11). (A) $Fr_1 = 7.6$. (B) $Fr_1 = 8.3$.

profiles exhibited a similar shape despite some data scatter. The data suggested further that the boundary layer thickness grew with the distance to the toe, while the maximum interfacial velocity decreased with increasing distance from the jump toe $(x − x_1)/d_1$. Following the work of Rajaratnam (1965) in monophase flows, Chanson and Brattberg (2000) showed that the dimensionless distributions of interfacial velocities were best fitted by some wall jet equations:

$$\frac{V}{V_{max}} = \left(\frac{y}{y_{V_{max}}}\right)^{1/N} \quad \text{for } \frac{y}{y_{V_{max}}} < 1 \tag{10}$$

$$\frac{V}{V_{max}} = \exp\left(-\frac{1}{2} \times \left[1.765\left(\frac{y - y_{V_{max}}}{y_{0.5}}\right)\right]^2\right)$$

$$\text{for } 1 < \frac{y}{y_{V_{max}}} < 3 \text{ to } 4 \tag{11}$$

where V_{max} is the maximum velocity measured at $y = y_{V_{max}}$, $y_{0.5}$ is the vertical elevation where $V = V_{max}/2$ and N is a constant ($N \approx 6$). Eqs. (10) and (11) are compared with the data in Fig. 11 and experimental observations of V_{max} and $y_{V_{max}}$ are reported in Table 2. The present results followed the wall jet velocity profile despite some data scatter caused by the unsteady and fluctuating nature of the flow.

The maximum velocity data V_{max} showed a gradual decrease with increasing distance from the jump toe. They compared favourably with the observations of Chanson and Brattberg (2000) (Fig. 12). All the data followed closely the empirical correlation:

$$\frac{V_{max}}{V_1} = \exp\left(-0.02875 \frac{x - x_1}{d_1}\right) \tag{12}$$

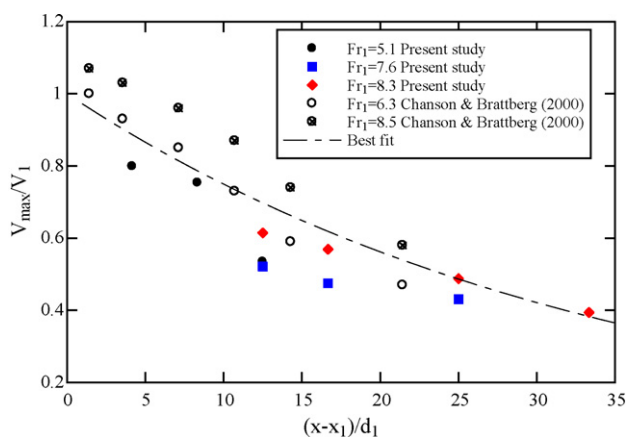Eq. (12) is compared with the experimental data in Fig. 12.

Fig. 12 – Longitudinal distribution of dimensionless maximum velocity V_{max}/V_1 in hydraulic jumps. Comparison with the data of Chanson and Brattberg (2000) and Eq. (12).

4. Conclusion

The hydraulic jump is a fascinating two-phase flow situation despite nearly two centuries of studies. Herein new series of experimental measurements were conducted in hydraulic jumps with Froude numbers between 5 and 8.5, and inflow Reynolds numbers between 38,000 and 62,000. The vertical profiles of void fraction showed two distinct regions, namely the turbulent shear region in the lower part of the flow and an upper free-surface region. In the air–water shear region, the void fraction and bubble count rate distributions exhibited marked peaks C_{max} and F_{max} respectively. The maximum of void fraction C_{max} was always found above the location of the maximum bubble count rate F_{max}. The quantitative values were functions of both Froude number and streamwise position, illustrating the influence of the Froude number on the air entrainment processes. Further, the dimensionless turbulent diffusivity estimates were comparable with previous studies. The data analysis showed also that the mean bubble chord length in the turbulent shear layer was between 1 mm and 6 mm. These basics results were in good agreement with previous experimental studies. The dimensionless distributions of interfacial velocity compared favourably with some wall-jet flow equations. The probability distribution functions (PDF) of bubble chord time illustrated a broad spectrum with predominance to small bubble chord times (less than 2–3 ms).

It is believed that the present results bring new information on the fluid dynamics of hydraulic jumps. They revealed the turbulent nature of this complex two-phase flow. The results will need further developments. For instance, experimental studies with larger Froude numbers could be undertaken as well as some analysis of bubble clustering and numerical studies.

Acknowledgments

References

Belanger, J.B., (1828). *Essai sur la Solution Numérique de quelques Problèmes Relatifs au Mouvement Permanent des Eaux Courantes.*

('Essay on the Numerical Solution of Some Problems relative to Steady Flow of Water'). (Carilian-Goeury, Paris, France) (in French)

Chanson, H., 1995, Air entrainment in two-dimensional turbulent shear flows with partially developed inflow conditions. Int J Multiphase Flow, 21(6): 1107–1121.

Chanson, H., (1997). *Air bubble entrainment in free-surface turbulent shear flows.* (Academic Press, London, UK), 401 p

Chanson, H., 2002, Air–water flow measurements with intrusive phase-detection probes. Can we improve their interpretation? J Hydraulic Eng-ASCE, 128(3): 252–255.

Chanson, H., (2004). *The Hydraulics of Open Channel Flows: An Introduction* (2nd edition). (Butterworth-Heinemann, Oxford, UK), 630 p

Chanson, H., 2005a, Physical modelling of the flow field in an undular tidal bore. J Hyd Res IAHR, 43(3): 234–244.

Chanson, H., 2005b, Air–water and momentum exchanges in unsteady surging waters: an experimental study. Exp Thermal Fluid Sci, 30(1): 37–47.

Chanson, H., 2007, Bubbly Flow Structure in Hydraulic Jump. Eur J Mech B/Fluids, 26(3): 367–384. doi:10.1016/j.euromechflu.2006.08.001

Chanson, H. and Brattberg, T., 2000, Experimental study of the air–water shear flow in a hydraulic jump. Int J Multiphase Flow, 26(4): 583–607.

Chanson, H. and Carosi, G., 2007, Turbulent time and length scale measurements in high-velocity open channel flows. Exp Fluids, 42(3): 385–401. doi:10.1007/s00348-006-0246-2

Crowe, C., Sommerfield, M. and Tsuji, Y., (1998). *Multiphase Flows with Droplets and Particles.* (CRC Press, Boca Raton, USA), 471 p

Gualtieri, C. and Chanson, H., 2007, Experimental analysis of Froude number effect on air entrainment in the hydraulic jump. Environ Fluid Mech, 7(3): 217–238. doi:10.1007/s10654-006-9016-1

Henderson, F.M., (1966). *Open Channel Flow.* (MacMillan Company, New York, USA).

Kalinske, A.A. and Robertson, J.M., 1943, Closed conduit flow. Transactions, ASCE, 108: 1435–1447.

Kucukali, S., and Chanson, H., 2007, "Turbulence in Hydraulic Jumps: Experimental Measurements." *Report No. CH62/07*, Div. of Civil Engineering, The University of Queensland, Brisbane, Australia, July, 96 pages.

Mossa, M. and Tolve, U., 1998, Flow visualization in bubbly two-phase hydraulic jump. J Fluids Eng ASME, 120(March): 160–165.

Murzyn, F., and Chanson, H., 2007, "Free Surface, Bubbly flow and Turbulence Measurements in Hydraulic Jumps." *Report CH63/07*, Div. of Civil Engineering, The University of Queensland, Brisbane, Australia, August, 114 p.

Murzyn, F., Mouaze, D. and Chaplin, J.R., 2005, Optical fibre probe measurements of bubbly flow in hydraulic jumps. Int J Multiphase Flow, 31(1): 141–154.

Murzyn, F., Mouaze, D. and Chaplin, J.R., 2007, Air–water interface dynamic and free surface features in hydraulic jumps. J Hydraulic Res IAHR, 45(5): 679–685.

Rajaratnam, N., 1962, An experimental study of air entrainment characteristics of the hydraulic jump. J Inst Eng India, 42(March (7)): 247–273.

Rajaratnam, N., 1965, The hydraulic jump as a wall jet. J Hyd Div ASCE, 91(HY5): 107–132 (Discussion: 92(HY3): 110–123; 93(HY1): 74–76)

Resch, F.J. and Leutheusser, H.J., 1972, Le Ressaut Hydraulique: mesure de Turbulence dans la Région Diphasique." ('The Hydraulic Jump: Turbulence Measurements in the Two-Phase Flow Region.'). Jl La Houille Blanche, (4): 279–293 (in French)

Wisner, P., 1965, Sur le Rôle du Critère de Froude dans l'Etude de l'Entraînement de l'Air par les Courants à Grande Vitesse. ('On the Role of the Froude Criterion for the Study of Air Entrainment in High Velocity Flows.'), In *Proc. 11th IAHR Congress* Leningrad, USSR, (p. 1.15) (in French)